JMEPEG (2008) 17:894–901
DOI: 10.1007/s11665-008-9247-z

1059-9495/$19.00

Strain Hardening and Strain-Rate Sensitivity of an Extruded Magnesium Alloy

X.Z. Lin and D.L. Chen

(Submitted December 30, 2007)

The strain-hardening behavior and strain-rate sensitivity of an extruded AZ31B magnesium alloy were determined at different strain rates between 10^{-2} and 10^{-5} s^{-1} in relation to the thickness of specimens (2.5 and 4.5 mm). Both the common approach and Lindholm's approach were used to evaluate the strain-rate sensitivity. The yield strength (YS) and the ultimate tensile strength (UTS) increased, the ductility decreased, and the brittle fracture characteristics increased with increasing strain rate. The thinner specimens exhibited a slightly higher UTS, lower ductility, higher strain-hardening exponent, and strain-hardening rate due to smaller grain sizes. The stage III strain-hardening rate linearly decreased with increasing true stress, but increased with increasing strain rate. In comparison to the common approach, the Lindholm's approach was observed to be more sensitive in characterizing the strain-rate sensitivity due to larger values obtained. The thinner specimens also exhibited higher strain-rate sensitivity. As the true strain increased, the strain-rate sensitivity decreased.

Keywords grain size effect, magnesium alloy, microstructural characterization, strain-hardening exponent, strain-hardening rate, strain-rate sensitivity, tensile properties

1. Introduction

With the constant increase of oil and gas prices, the automotive and aerospace industry constantly seeks lightweight materials that enable the replacement of heavier components, so as to manufacture lighter vehicle and cut the costs for both consumers and manufacturers, and ultimately improve fuel efficiency and reduce greenhouse gas emissions. The application of magnesium alloys is a major consideration in the recent automotive and aerospace development due to their high strength-to-weight ratio, environmental friendliness, recyclability, and castability (Ref 1). In these structural applications, it is necessary to evaluate the mechanical properties and deformation characteristics of magnesium alloys, such as, strain-hardening exponent, strain-hardening rate, and strain-rate sensitivity.

The strain-rate sensitivity and strain-hardening rate are observed to be associated with a number of parameters such as the specimen geometry (Ref 2-4), grain size (Ref 4-7), strain level (Ref 8-13), and strain rate (Ref 8-17). Some inconsistent results regarding the effect of these parameters have been reported in the literature. Chin and Yi (Ref 3) conducted constant crosshead speed tensile testing on a Zn-5Al eutectic alloy, and reported that as the strain increased, the strain-rate sensitivity first increased and then decreased, i.e., a maximum value of strain-rate sensitivity was obtained as a function of the strain level. On the other hand, Jain et al. (Ref 8) conducted constant strain rate tests in Ti-6Al-4V sheet alloy at different strain rates, and found that as the strain increased, the strain-rate sensitivity decreased. Subsequently, Jiang et al. (Ref 14) tensile tested AM30 magnesium alloy at different temperatures with different strain rates, and observed that as the strain rate increased the strain-hardening exponent, n, decreased at room temperature. However, Takuda et al. (Ref 15) tensile tested Mg-9Li-1Y alloy at room temperature and observed an increase of the n value with increasing strain rate. Recently, del Valle et al. (Ref 18) observed that decreasing grain size corresponded to a decrease in the strain-hardening rate ($\theta = d\sigma/d\varepsilon$) in AZ31 magnesium alloy after annealing treatments to produce grain sizes from ~2 to 55 μm (Ref 6, 18). If the Haasen plot of the strain-rate sensitivity parameter (defined as $\partial\sigma/\partial \ln \dot{\varepsilon}$) as a function of the flow stress was used, a strong increase in the strain-rate sensitivity with decreasing grain size was observed (Ref 6). While a close correlation between the strain-rate sensitivity and the work-hardening behavior was observed, the existing models were pointed out to be unable to explain the grain size dependence (Ref 6, 18). It can be seen that the strain-hardening behavior and strain-rate sensitivity in characterizing the deformation behavior of magnesium alloys have not been fully understood. The aim of this study was, therefore, to evaluate the strain-hardening behavior and the strain-rate sensitivity in relation to the effect of the specimen thickness and microstructure of an extruded AZ31B magnesium alloy.

2. Experimental Procedures

Extruded rectangular magnesium alloy AZ31B (2.5-3 wt.% Al, 0.9-1 wt.% Zn, and balance Mg) bar with a thickness of 4.5 mm and width of 47.5 mm on the shorter side of the rectangle, and a thickness of 2.5 mm and width of 91.8 mm on the longer side of the rectangle was received from Timminco

X.Z. Lin, D.L. Chen, and , Department of Mechanical and Industrial Engineering, Ryerson University, 350 Victoria Street, Toronto, ON, Canada M5B 2K3. Contact e-mail: dchen@ryerson.ca.

Metals via CANMET-Materials Technology Laboratory (MTL), Ottawa, Canada. Metallographic samples in the longitudinal (L), transverse (T), and short transverse (S) were cut for both thicker and thinner portions. The samples were cold-mounted with LECO 7007 resin powder and liquid, then ground with SiC sand papers of different grades with water as the lubricant and ethanol to clean it in each step. Polishing was done with 6 μm, 3 μm, and then 1 μm diamond paste, using the diamond extender as lubricant. After the final polishing with the Masterprep solution, the samples were etched with the picric acid reagent consisting of 4.2 g picric acid, 10 mL acetic acid, 10 mL H_2O, and 70 mL ethanol (95% concentration). The microstructure was observed with a light microscope equipped with quantitative image analysis software.

Vickers microhardness tests were conducted with a computerized Buehler machine along the thickness direction of the cut specimens in an increment of 0.2 mm. A load of 50 g and a dwell time of 15 s were applied during the hardness tests. Subsized tensile specimens in accordance with ASTM E8 standard were machined along the extrusion or longitudinal direction for both the thinner and thicker part of the extruded rectangular bar. The gage area was ground with SiC papers up to #800. Tensile tests were conducted at a constant strain rate of 10^{-2}, 10^{-3}, 10^{-4}, and 10^{-5} s^{-1} at room temperature. Strain-hardening rate was plotted as a function of true stress (σ) to identify the strain hardening stages. The strain-rate sensitivity was evaluated from the tensile test results in two ways. In the common approach (Ref 19), the slope in the plot of $\ln \sigma$ vs. $\ln \dot{\varepsilon}$ was used to represent the strain-rate sensitivity. The other method for the evaluation of the strain-rate sensitivity was the Lindholm approach (Ref 20), which corresponded to the slope of the graph of σ vs. $\log \dot{\varepsilon}$. The fracture surfaces were examined using a scanning electron microscope (SEM) equipped with an energy dispersive X-ray spectroscopy (EDS) system.

3. Results and Discussion

Figure 1 shows the microstructure of the thinner (2.5 mm) and thicker (4.5 mm) sheet samples of the extruded AZ31B alloy in the longitudinal (L), transverse (T), and short transverse (S) directions. As seen from the figure, the thicker portion of the extruded bar had a larger average grain size than the thinner portion, which was related to the process of producing the material. During cooling of the extruded bar, the thicker part would experience a slower cooling rate (Ref 21). This allowed a longer time for the dynamic recrystallization and grain growth in the thicker portion. SEM/EDS revealed that the small micron-sized particles were Mn-containing inclusions. It can also be seen that somewhat elongated grains appeared in the longitudinal and transverse directions. The average grain size and microhardness values for both thinner and thicker samples are given in Table 1. Since the thicker samples had bigger grain sizes, the microhardness became slightly lower.

Figure 2 shows true stress-strain curves of the AZ31B magnesium alloy tested at different strain rates. As the strain rate increased, the flow curves shifted higher, giving rise to a higher yield strength (YS) and ultimate tensile strength (UTS). Similar results have been reported for AM30 (Ref 14), AZ31B-H24 (Ref 22, 23), cryo-rolled Cu (Ref 17), and Mg-9Li-1Y alloy (Ref 15). The yield strength, ultimate tensile strength, and ductility as a function of strain rate are shown in Fig. 3 for both thinner and thicker specimens. It is seen that both the YS and UTS increased linearly with increasing strain rate in the double-log scales, while the ductility decreased as the strain rate increased. Therefore, the effect of the strain rate on the flow stress of AZ31B extruded alloy can be well described using a power law (Ref 24),

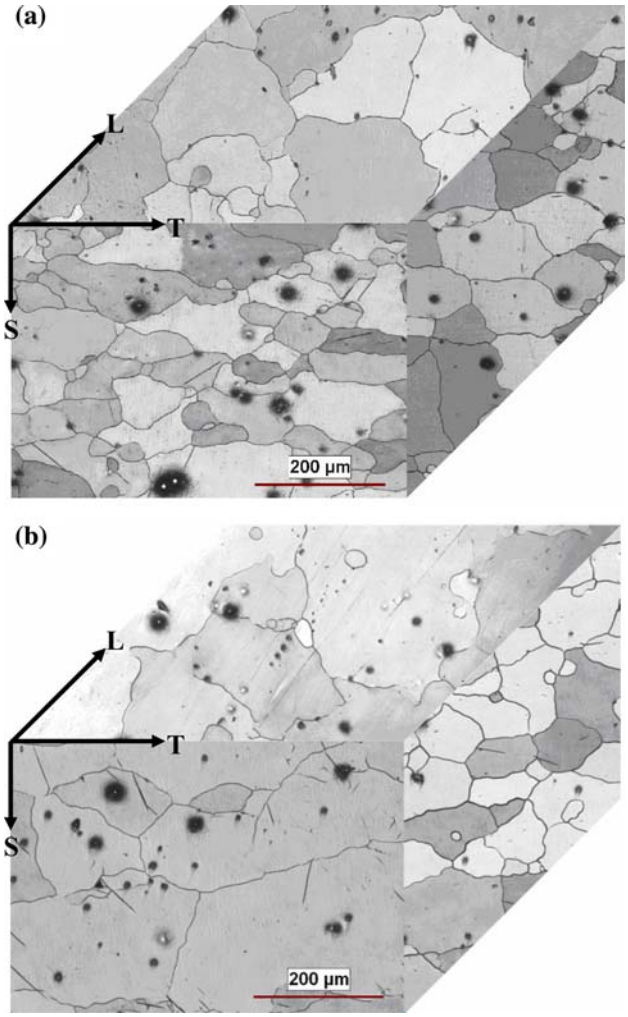

Fig. 1 Microstructure of (a) thinner sheet and (b) thicker sheet in the longitudinal (L), transverse (T), and short transverse (S) directions

Table 1 Average grain size and microhardness values for both thinner (2.5 mm) and thicker (4.5 mm) specimens taken from a rectangular bar of extruded AZ31B magnesium alloy

Specimen	Grain size, μm	Microhardness, HV
Thinner-L	47	34
Thinner-ST	51	
Thinner-T	51	
Thicker-L	104	33
Thicker-ST	87	
Thicker-T	56	

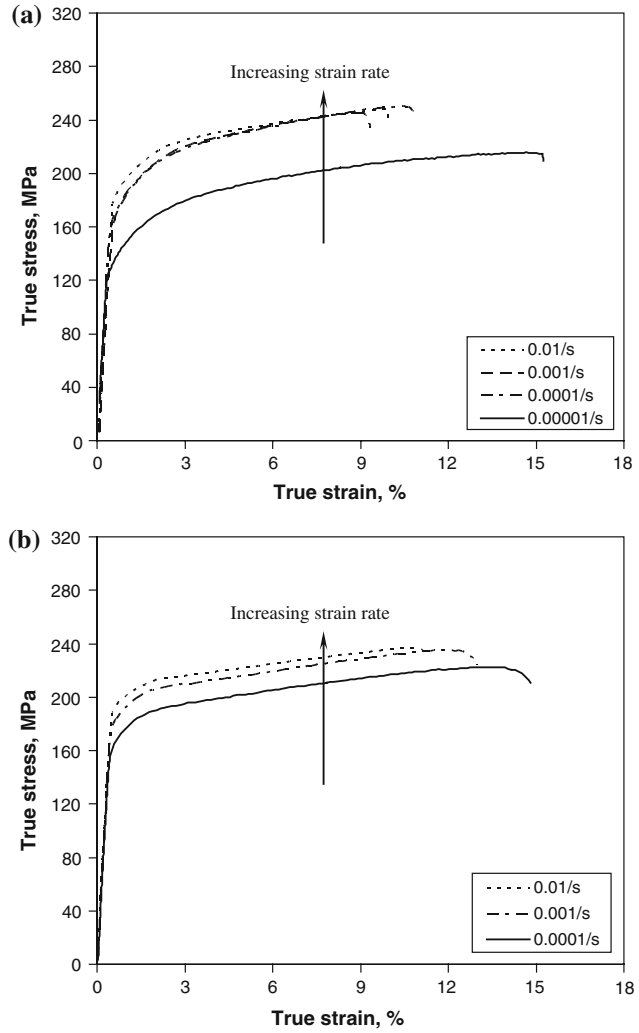

Fig. 2 True stress-strain curves at different strain rates for (a) thinner and (b) thicker specimens

$$\sigma = C\dot{\varepsilon}^{m}, \qquad \text{(Eq 1)}$$

where σ is the flow stress, C is a constant, and m is the strain-rate sensitivity.

As seen from Fig. 3(c), the thicker specimens exhibited a higher ductility than the thinner specimens. This could be understood through the effect of specimen thickness on the toughness. Pardoen et al. (Ref 25, 26) and Bluhm (Ref 27) presented fracture/thickness curve from tensile tests on cracked specimens, and observed that the increase of specimen thickness increased the fracture toughness for the thickness in the range of 1-6 mm (Ref 25-28). Chin and Yi (Ref 3) also reported that for Zn-5Al alloy with increasing thickness from 1 to 2 mm, the percent elongation (ductility) increased. Asserin-Lebert et al. (Ref 2) tensile tested both cracked and uncracked 6056 aluminum samples and further verified the above observation, and showed that the elongation increased with increasing specimen thickness of 1.4, 3.2, and 6.0 mm. This is related to the structural stability of the specimen, as it is quite low for thin specimens (Ref 2, 29).

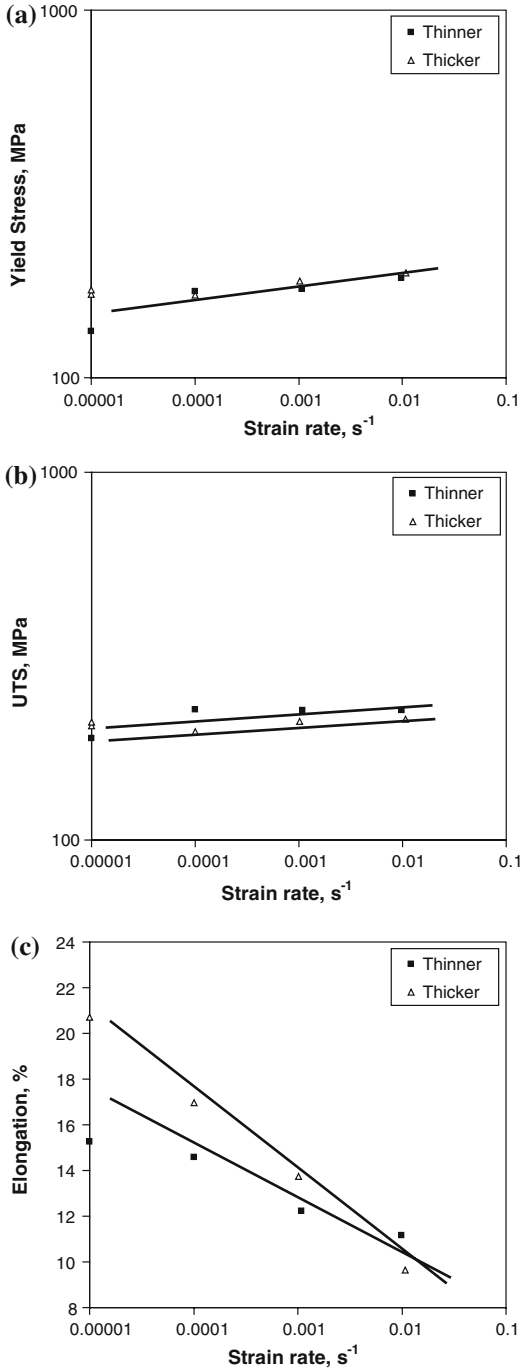

Fig. 3 (a) Yield strength (YS), (b) ultimate tensile strength (UTS), and (c) ductility of the thinner and thicker specimens as a function of the strain rate

The following Hollomon equation,

$$\sigma = K\varepsilon^{n}, \qquad \text{(Eq 2)}$$

has been suggested in ASTM E646 to describe approximately the flow curve in the uniform deformation stage, where K is the strength coefficient and n is the strain-hardening exponent. The n values evaluated on the basis of Eq 2 as a function of the strain rate is shown in Fig. 4 for both thinner and thicker specimens. It is seen that the n values decreased linearly with increasing strain rate in the semi-log scale, which

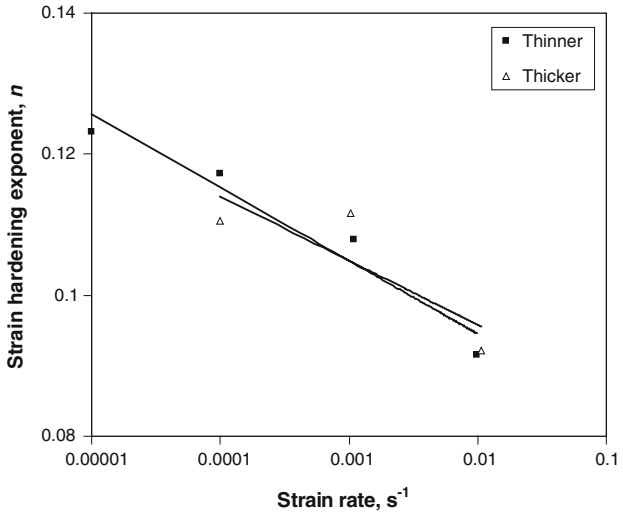

Fig. 4 Effect of strain rate ($\dot{\varepsilon}$) on the strain-hardening exponent, n, for the thicker and thinner specimens

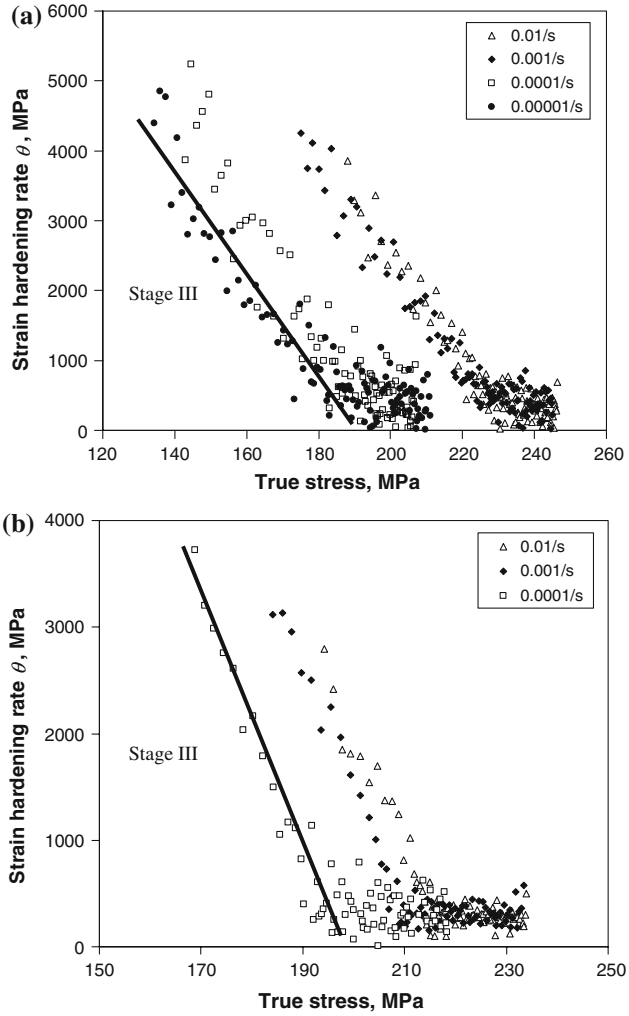

Fig. 5 Strain-hardening rate vs. true stress at different strain rates for (a) thinner and (b) thicker specimens

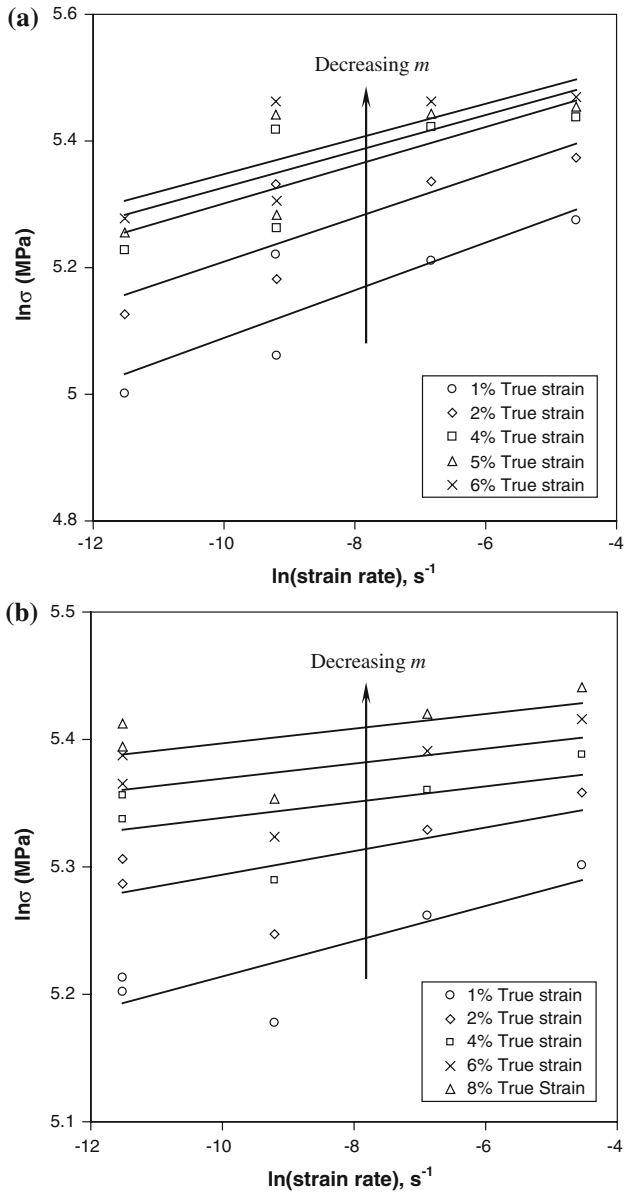

Fig. 6 The plot used to evaluate the strain-rate sensitivity index, m, at different true strain values via the common approach for (a) thinner and (b) thicker specimens

was also observed to be the case by Tang et al. (Ref 30) for four metallic materials, and 18%Ni 300 steel (Ref 31) and Ti-6Al-4V alloy (Ref 32). This could be expressed using an equation reported by Tang et al. (Ref 30),

$$n = n_0 - b \log \dot{\varepsilon}, \qquad \text{(Eq 3)}$$

where n is the strain-hardening exponent, n_0 is a constant, and b is the slope in the n vs. $\log \dot{\varepsilon}$ graph. The linear decrease of n values with increasing strain rate in the log-scale shown in Fig. 4 is also in good agreement with the results obtained in AM30 magnesium alloy tested at 25 °C (Ref 14, 16, 33), due to the softening effect of $\{10\bar{1}1\} - \{10\bar{1}2\}$ double twinning and $\{10\bar{1}1\}$ contraction twinning (Ref 16).

As shown in Fig. 4, the thinner specimens seemed to have a slightly higher strain-hardening exponent than the thicker specimens at lower strain rates. The strain hardening could be understood on the basis of the relationship involving the grain

size strengthening and dislocation strain hardening (Ref 21, 23). The following equation has been given by del Valle et al. (Ref 6, 18),

$$\sigma = \sigma_0 + \sigma_{HP} + \sigma_d, \quad \text{(Eq 4)}$$

where σ_0 is a frictional contribution, $\sigma_{HP} = kd^{-1/2}$ is the Hall-Petch contribution $\sigma_d = M\alpha Gb\rho^{1/2}$ is the Taylor dislocation contribution, M is the Taylor factor, α is a constant, G is the shear modulus, b is the Burgers vector, and ρ is the total dislocation density. Equation 4 shows that with decreasing grain size d, the Hall-Petch contribution increased due to dislocation-grain boundary interactions (Ref 34). Strain hardening of a material in stage III is sensitive to the dislocation strain field interactions, hence the Taylor dislocation contribution in Eq 4 is significant (Ref 23, 35). As the number of dislocations increased during deformation, the spacing among them became smaller and their interactions were more repulsive, which ultimately increased the resistance to deformation. The effect of grain size on the strain hardening was indeed complicated. While the Hall-Petch contribution increased with decreasing grain size, the reduction in the grain size might limit the storage of dislocations within grains since the dislocation accumulation rate was inversely proportional to the mean free path (Ref 35), and the presence of grain boundaries restricted the mean free path of dislocations (Ref 36). It has been reported that at lower strains the grain size had a strong contribution to the strain hardening, and the influence of the grain size on the strain hardening was assumed to vanish at larger strains due to dislocation screening and dynamic recovery effects at grain boundaries (Ref 34, 37). However, as seen in Fig. 4 with increasing strain rates the difference in the strain-hardening exponents between the thicker and thinner specimens became negligible.

Figure 5 shows a typical Kocks-Mecking plot of strain hardening rate ($\theta = d\sigma/d\varepsilon$) vs. true stress ($\sigma$) for AZ31B extruded magnesium alloy tested at different strain rates. The linear decrease in the strain-hardening rate indicates stage III hardening (Ref 35, 38). In this stage dynamic recovery occurs as the stress has reached a point that dislocation annihilations take place (Ref 19). The work-hardening rate would ultimately decrease to about 0 MPa (Ref 7, 11). Figure 5 also shows that the strain-hardening rate increases with increasing strain rate.

Table 2 Strain-rate sensitivity values for the thinner and thicker specimens, evaluated with the common approach (m) and Lindholm's approach (m_L)

	True strain, %	m	m_L
Thinner sheet	1	0.038	14.84
	2	0.035	15.29
	4	0.030	14.48
	5	0.029	14.07
	6	0.028	13.80
Thicker sheet (a)	1	0.0138	6.07
	2	0.0093	4.39
	4	0.0062	3.04
	6	0.0059	2.97
	8	0.0057	2.97

(a) The fourth decimal place for m is used to show the small difference at larger true strain values

This can be explained on the basis of the following equation (Ref 35, 39),

$$\theta = \theta_0 - \frac{R_d\sigma}{\dot{\varepsilon}^{1/q}}, \quad \text{(Eq 5)}$$

where R_d and q are temperature dependent, but are independent of stress and strain rate (Ref 35), which are constants in this study. θ is the strain-hardening rate in stage III, and θ_0 is considered as a constant. It is evident that as the strain rate increases, the strain-hardening rate θ increases. It can be seen from Fig. 5 that the thinner specimens have a higher strain-hardening rate than the thicker specimens. This would be attributed to the effect of the grain size on the strain-hardening rate. The increase of strain-hardening rate with decreasing grain size was also reported in cadmium by Risebrough and Teghtsoonian (Ref 40), due to either higher hardening rate of the nonbasal

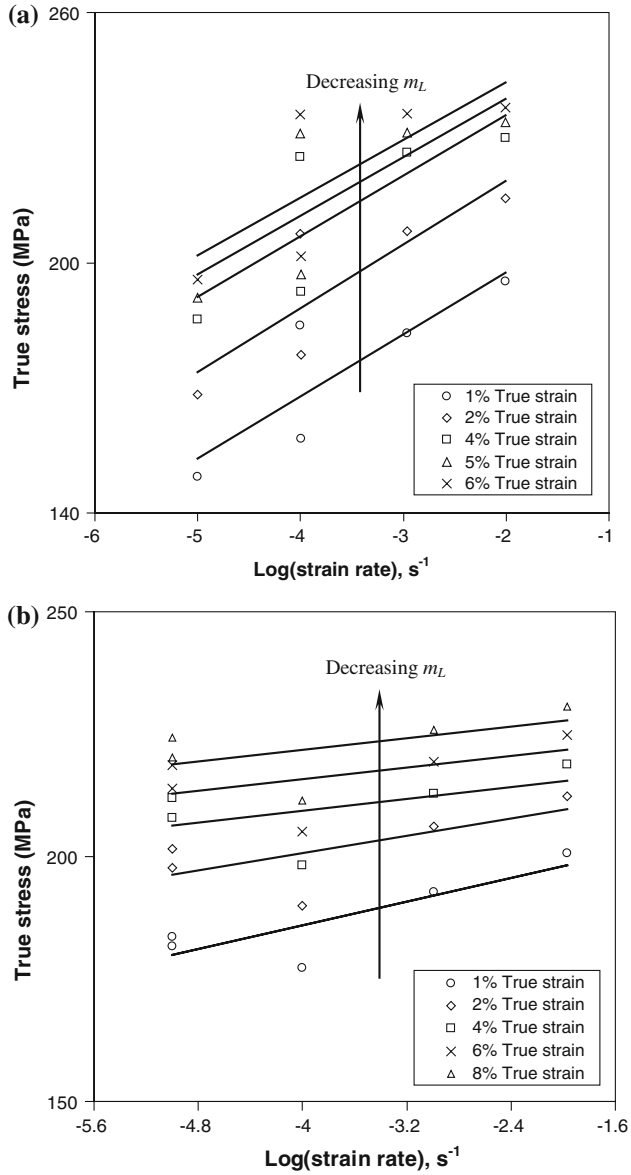

Fig. 7 The plot used to evaluate the strain-rate sensitivity index, m_L, at different true strain values via the Lindholm's approach for (a) thinner and (b) thicker specimens

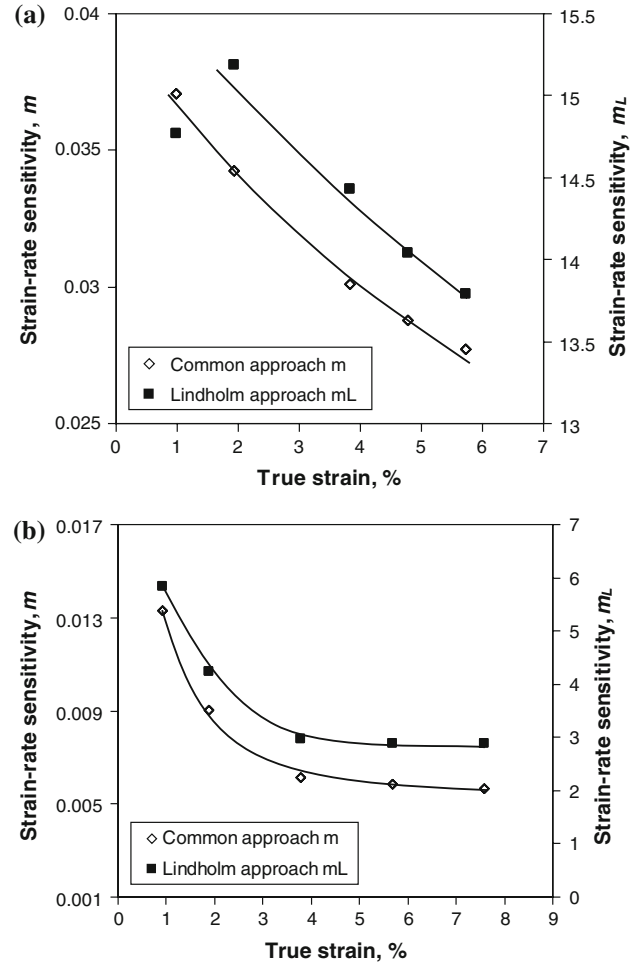

Fig. 8 Comparison between the strain rate-sensitivity values evaluated using the common approach and Lindholm's approach for (a) thinner and (b) thicker specimens

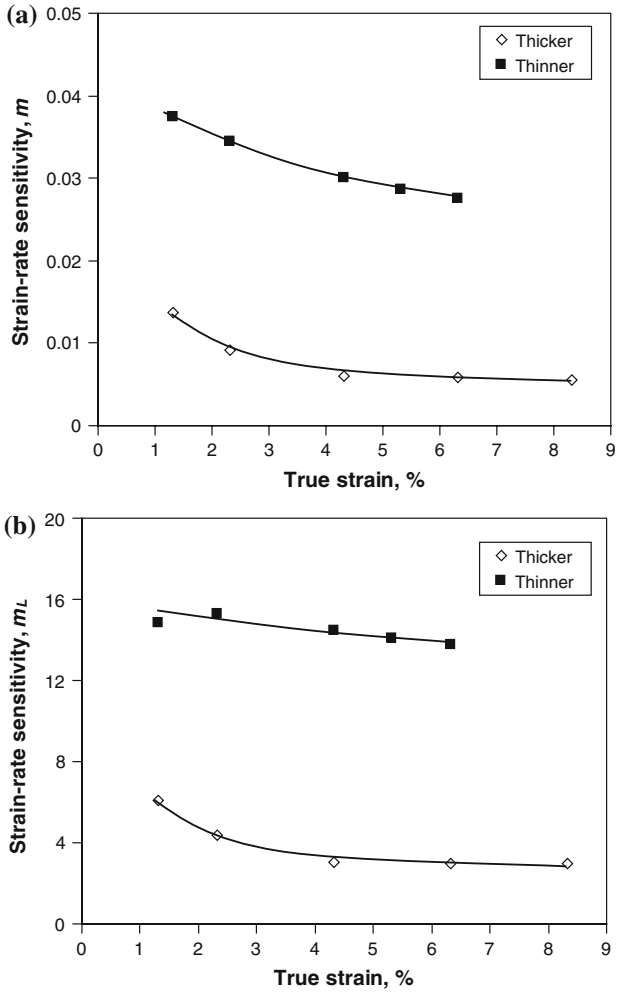

Fig. 9 Strain-rate sensitivity as a function of true strain for the thinner and thicker specimens evaluated using (a) common approach and (b) Lindholm's approach

system or an increase in forest dislocation density through the motion of the basal dislocations; it is, however, difficult to identify one sole contribution (Ref 40).

Another important parameter involving the deformation behavior of materials is the strain-rate sensitivity, m. Plots based on Eq 1 at certain true strains within the YS and UTS are shown in Fig. 6. The m values evaluated from the plots are listed in Table 2. As the true strain increases the strain-rate sensitivity decreases. Similar results were also reported in Ti-6Al-4V (Ref 8) and ultrafine-crystalline Cu (Ref 5). The Lindholm approach (Ref 20) was also used to evaluate the strain-rate sensitivity based on the following equation,

$$\sigma = \sigma_0(\varepsilon) + \sigma_1(\varepsilon)\log\dot{\varepsilon}. \qquad \text{(Eq 6)}$$

The Lindholm strain-rate sensitivity, m_L, is $\sigma_1(\varepsilon)$ in the equation. The plots of σ vs. $\log\dot{\varepsilon}$ at different true strain values are shown in Fig. 7 for the thinner and thicker specimens. The obtained m_L values are given in Table 2. Both strain-rate sensitivity values as a function of the true strain are shown in Figs. 8 and 9 for the thinner and thicker specimens. The Lindholm approach is observed to be more sensitive since it gives much larger values for both thinner and thicker specimens (Fig. 8). While the Lindholm strain-rate sensitivity values are much larger, both the common and Lindholm strain-rate sensitivity values decrease monotonically with increasing true strain. This is in agreement with the results reported in Ref 5 and 8. It is also seen from Table 2 and Fig. 9 that the thicker specimens exhibit a lower strain-rate sensitivity value, irrespective of the evaluation methods. This could be related to the difference in the microstructure. del Valle and Ruano (Ref 6) have recently reported a relationship among the stress, strain-rate sensitivity, and grain size as shown below,

$$\frac{\partial\sigma}{\partial\ln\dot{\varepsilon}} = \frac{k}{2}d^{-1/2}(M_c - 2M_{cg}) + \sigma M_{cg}, \qquad \text{(Eq 7)}$$

where k is Boltzmann constant, d is the grain size, σ is the flow stress, $M_{cg} = \partial\ln\sigma_{cg}/\partial\ln\dot{\varepsilon}$ and $M_c = \partial\ln\tau_c/\partial\ln\dot{\varepsilon}$. M_{cg} is considered as a constant because of the Cottrell-Stokes law (Ref 5, 41-43). This equation expresses a linear correlation between the strain-rate sensitivity, flow stress σ, and grain size in the form of $d^{-1/2}$. It means that the strain-rate sensitivity increases with decreasing grain size. Since the grain size is smaller (Table 1), the strain-rate sensitivity would be higher in the thinner specimens, as shown in Fig. 9 and Table 2.

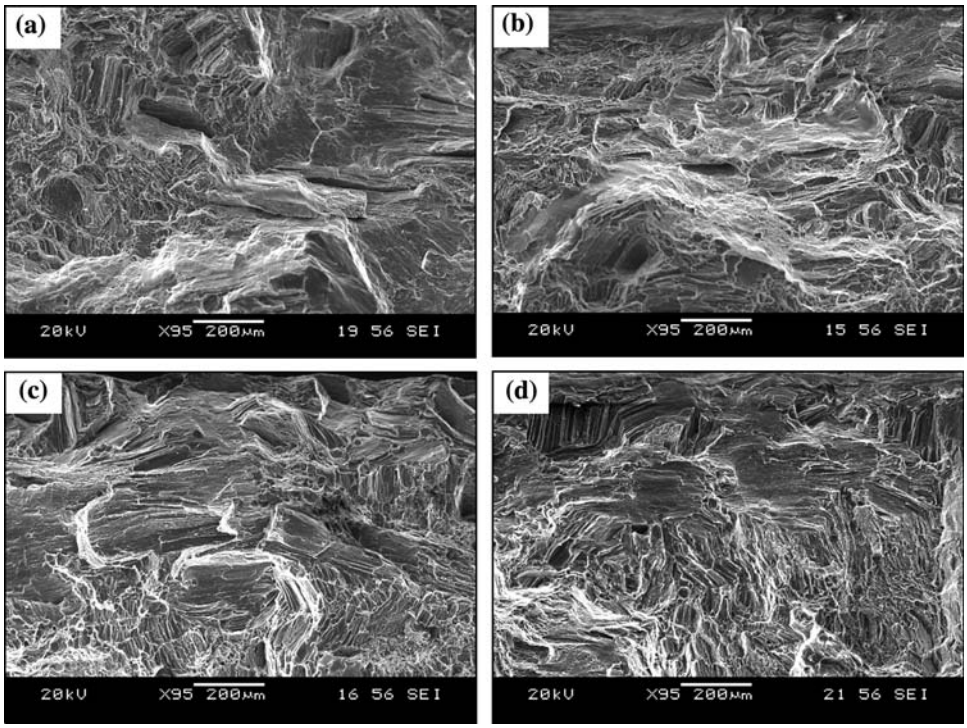

Fig. 10 SEM images showing the fracture surfaces of the thicker specimens tested at strain rates of (a) 10^{-2} s^{-1}, (b) 10^{-3} s^{-1}, (c) 10^{-4} s^{-1}, and (d) 10^{-5} s^{-1}

Figure 10 shows a typical example of the fracture surfaces of the thicker specimens tested at different strain rates between 10^{-2} and 10^{-5} s^{-1}. At the fastest strain rate, cleavage-like failure appeared more apparent. With decreasing strain rate, dimple-like ductile fracture appeared more evident. Similar fracture surface characteristics were observed in the thinner specimens. This is in agreement with the observations on the effect of strain rate in 18%Ni 300 maraging steel sheet (Ref 31). Secondary cracks and tear ridges were also observed on the fracture surfaces. Although some inclusions were present in the AZ31B extruded magnesium alloy (Fig. 1), crack initiation during the tensile tests occurred basically from the specimen surface.

4. Conclusions

1. Microstructural examination of AZ31B extruded magnesium alloy revealed a larger grain size in the thicker part than in the thinner part, as the thicker part experienced a lower cooling rate and hence a longer time for recrystallization and grain growth immediately after extrusion.
2. Tensile test results showed an increase of the yield strength (YS) and ultimate tensile strength (UTS) and a decrease of the ductility with increasing strain rate. Despite little difference in YS, the thicker specimens exhibited lower UTS than the thinner specimens.
3. In comparison with the thinner specimens, the thicker specimens displayed a slightly lower strain-hardening exponent and strain-hardening rate. The strain-hardening rate increased with increasing strain rate at a given flow stress.
4. Both the common approach and Lindholm's approach on the evaluation of the strain-rate sensitivity revealed similar results. The thicker specimens with bigger grain sizes had a lower strain-rate sensitivity value than the thinner specimens. The Lindholm's approach was observed to be more sensitive since it gave larger values. The strain-rate sensitivity decreased with increasing true strain.
5. Dimple-like ductile fracture, coupled with tear ridges and secondary cracks, was observed to be the main feature on the fracture surfaces. As the strain rate increased, more cleavage-like features appeared. The crack initiation basically occurred from the specimen surface.

Acknowledgments

The authors would like to thank the National Sciences and Engineering Research Council of Canada (NSERC) and AUTO21 Network of Centres of Excellence for providing financial support, and Timminco Metals for providing the test material in this study via CANMET-Materials Technology Laboratory (MTL), Ottawa, Canada. This investigation involves part of Canada-China-USA Collaborative Research Project on the Magnesium Front End Research and Development (MFERD), and financial support from CANMET-MTL is acknowledged. One of the authors (D.L. Chen) is also grateful for the financial support by the Premier's Research Excellence Award (PREA), Canada Foundation for Innovation (CFI), and Ryerson Research Chair (RRC) program. Dr. A.A. Luo (GM), Dr. S. Xu, Dr. K. Sadayappan, Dr. J. Lo, and Dr. J. Jackman (CANMET-MTL) are gratefully acknowledged for the helpful discussion and continuous encouragement while performing this investigation. The authors would also like to thank Messrs. A. Machin, Q. Li, J. Amankrah, and R. Churaman for easy access

to the laboratory facilities of Ryerson University and their assistance in the experiments.

References

1. A. Tharumarajah and P. Koltun, Is there an Environmental Advantage of Using Magnesium Components for Light-Weighting Cars?, *J. Clean. Prod.*, 2007, **15**(11–12), p 1007–1013
2. A. Asserin-Lebert, J. Besson, and A.F. Gourgues, Fracture of 6056 Aluminum Sheet Materials: Effect of Specimen Thickness and Hardening Behavior on Strain Localization and Toughness, *Mater. Sci. Eng. A*, 2005, **395**(1–2), p 186–194
3. L. Chin and S.G. Yi, Chin Liu Strain Rate Sensitivity Index – Strain Equation of Superplasticity and Influence of Specimen Geometry, *Mater. Sci. Technol.*, 1990, **6**(2), p 141–145
4. N. Igata, K. Miyahara, T. Uda, and S. Asada, Effects of Specimen Thickness and Grain Size on the Mechanical Properties of Types 304 and 316 Austenitic Stainless Steel, *ASTM Special Technical Publication*, 1986, p 161–170
5. Y.F. Shen, L. Lu, M. Dao, and S. Suresh, Strain Rate Sensitivity of Cu with Nanoscale Twins, *Scripta Mater.*, 2006, **55**(4), p 319–322
6. J.A. del Valle and O.A. Ruano, Influence of the Grain Size on the Strain Rate Sensitivity in an Mg-Al-Zn Alloy at Moderate Temperatures, *Scripta Mater.*, 2006, **55**(9), p 775–778
7. Y.M. Wang and E. Ma, Strain Hardening and Strain Rate Sensitivity of Ultrafine-Grained Metals, *J. Metastable Nanocryst. Mater.*, 2003, **17**, p 55–65
8. M. Jain, M.C. Chaturvedi, N.L. Richards, and N.C. Goel, Strain Rate Sensitivity Effects with Forming Characteristics of Superplastic Ti-6Al-4V, *Mater. Sci. Eng. A*, 1991, **A138**(2), p 205–211
9. X. Yao and S. Zajac, The Strain-Rate Dependence of Flow Stress and Work-Hardening Rate in Three Al-Mg Alloys, *Scand. J. Metall.*, 2000, **29**(3), p 101–107
10. L. Blaz and E. Evangelista, Strain Rate Sensitivity of Hot Deformed Al and AlMgSi Alloy, *Mater. Sci. Eng. A*, 1996, **A207**(2), p 195–201
11. C.P. Ling and P.G. McCormick, Effect of Temperature on Strain Rate Sensitivity in an Al-Mg-Si Alloy, *Acta Metall. Mater.*, 1993, **41**(11), p 3127–3131
12. A. Melander and A. Thuvander, Diffuse Necking in Sheet Tensile Specimens, *Res Mech.*, 1982, **5**(2), p 129–149
13. F.U. Enikeev, Strain-Rate Sensitivity Index *m*: Definition, Determination, Narrowness, *Mater. Sci. Forum*, 1997, **243–245**, p 77–88
14. L. Jiang, J.J. Jonas, A.A. Luo, A.K. Sachdev, and S. Godet, Microstructure and Texture Evolution During the Uniaxial Tensile Testing of AM30 Magnesium Alloy, *Magnesium Technology*, A.A. Luo, N.R. Neelameggham, and R.S. Beals, Eds., TMS, Warrendale, PA, 2006, p 233–238
15. H. Takuda, S. Kikuchi, N. Yoshida, and H. Okahara, Tensile Properties and Press Formability of Mg-9Li-1Y Alloy Sheet, *Mater. Trans.*, 2003, **44**(11), p 2266–2270
16. L. Jiang, J.J. Jonas, A.A. Luo, A.K. Sachdev, and S. Godet, Twinning-Induced Softening in Polycrystalline AM30 Mg Alloy at Moderate Temperatures, *Scripta Mater.*, 2006, **54**, p 771–775
17. Y.M. Wang and E. Ma, Strain Hardening, Strain Rate Sensitivity, and Ductility of Nanostructured Metals, *Mater. Sci. Eng. A*, 2004, **A375–377**, p 46–52
18. J.A. del Valle, F. Carreno, and O.A. Ruano, Influence of Texture and Grain Size on Work Hardening and Ductility in Magnesium-Based Alloys Processed by ECAP and Rolling, *Acta Mater.*, 2006, **54**(16), p 4247–4259
19. G.E. Dieter, *Mechanical Metallurgy.* 3rd ed., McGraw-Hill, Boston, USA, 1986
20. U.S. Lindholm, Some Experiments with Split Hopkinson Pressure Bar, *J. Mech. Phys. Solids*, 1964, **12**(5), p 317–335
21. W.D. Callister Jr., *Materials Science and Engineering – An Introduction*. 7th ed., John Wiley & Sons, Inc., New York, USA, 2007
22. V. Livescu, C.M. Cady, E.K. Cerreta, B.L. Henrie, and G.T. Gray III, The High Strain Rate Deformation Behavior of High Purity Magnesium and AZ31B Magnesium Alloy, *Magnesium Technology*, A.A. Luo, N.R. Neelameggham, and R.S. Beals, Eds., TMS, Warrendale, PA, 2006, p 153–158
23. N. Afrin, D.L. Chen, X. Cao, and M. Jahazi, Strain Hardening Behavior of a friction Stir Welded Magnesium Alloy, *Scripta Mater.*, 2007, **57**, p 1004–1007
24. W.F. Hosford, *Mechanical Behavior of Materials*. Cambridge University Press, 2005
25. T. Pardoen, Y. Marchal, and F. Delannay, Thickness Dependence of Cracking Resistance in Thin Aluminum Plates, *J. Mech. Phys. Solids*, 1999, **47**(10), p 2093–2123
26. T. Pardoen, Y. Marchal, and F. Delannay, Essential Work of Fracture Compared to Fracture Mechanics – Towards a Thickness Independent Plane Stress Toughness, *Eng. Fract. Mech.*, 2002, **69**(5), p 617–31
27. J.I. Bluhm, A Model for the Effect of Thickness on Fracture Toughness, *ASTM Proc.*, 1961, **61**, p 1324–1331
28. Y. Bao, Dependence of Fracture Ductility on Thickness, *Thin-Walled Struct.*, 2004, **42**, p 1211–1230
29. A. Needleman and J. Rice, Limits to Ductility Set by Plastic Flow Localization, *Mechanics of Sheet Metal Forming*, D.P. Koistinen, Ed., Plenum Publishing Corporation, 1978, p 237–267
30. C.G. Tang, J.H. Zhu, Y.H. Zhang, and H.J. Zhou, Effect of Strain Rate $\dot{\varepsilon}$ on Strain Hardening Exponent n of Some Metallic Materials, *Acta Metall. Sinica*, 1994, **7**(3), p 183–186
31. A.A. Mazhar, E.A. Khorkhar, and A.Q. Khan, Effect of Strain Rate on Tensile Deformation and Fracture Behaviour of 18% Ni 300 Maraging Steel Sheet, *Mater. Sci. Technol.*, 1988, **4**(6), p 535–539
32. A. El-Domiaty, The Effect of Strain, Strain Rate and Temperature on Formability of Ti-6Al-4V Alloy, *J. Mater. Process. Technol.*, 1992, **32**(1–2), p 243–251
33. A.A. Luo and A. Sachdev, Mechanical Properties and Microstructure of AZ31 Magnesium Alloy Tubes, *Magnesium Technology*, A.A. Luo, Ed., TMS, Warrendale, PA, 2004, p 79–85
34. C.W. Sinclair, W.J. Poole, and Y. Brechet, A Model for the Grain Size Dependent Work Hardening of Copper, *Scripta Mater.*, 2006, **55**, p 739–742
35. U.F. Kocks and H. Mecking, Physics and Phenomenology of Strain Hardening: The FCC Case, *Prog. Mater. Sci.*, 2003, **48**(3), p 171–273
36. J.J. Gracio, The Double Effect of Grain Size on the Work Hardening Behaviour of Polycrystalline Copper, *Scripta Metall. Mater.*, 1994, **31**(4), p 487–489
37. I. Kovacs, N.Q. Chinh, and E. Kovacs-Csetenyi, Grain Size Dependence of the Work Hardening Process in Al99.99, *Phys. Status Solidi (a)*, 2002, **194**, p 3–18
38. J. Luo, Z. Mei, W. Tian, and Z. Wang, Diminishing of Work Hardening in Electroformed Polycrystalline Copper with Nano-Sized and Uf-Sized Twins, *Mater. Sci. Eng. A*, 2006, **441**, p 282–290
39. D. Kuhlmann-Wilsdorf, Theory of Work Hardening 1934–1984, *Metall. Trans. A*, 1985, **16A**, p 2091–2108
40. N.R. Risbrough and E. Teghtsoonian, The Linear Hardening of Cadmium, *Can. J. Phys.*, 1967, **45**(2), p 591–605
41. J. Gil Sevillano, Flow Stress and Work Hardening, *Materials and Technology: Plastic Deformation and Fracture of Materials*, Vol. 6, H. Mughrabi, Ed., VCH Publishers, New York, 1993, p 19–88
42. B.J. Diak, K.R. Upadhyaya, and S. Saimoto, Characterization of Thermodynamic Response by Materials Testing, *Prog. Mater. Sci.*, 1998, **43**(4), p 223–363
43. U.F. Kocks, A.S. Argon, and M.F. Ashby, Thermodynamics and Kinetics of Slip, *Prog. Mater. Sci.*, 1975, **19**, p 1–291